Quantitative magnetic resonance imaging of in vitro gastrointestinal digestion of a bread and cheese meal

Maja Musse, Steven Le Feunteun, Guylaine Collewet, Sylvain Challois, Mattéi Ravilly, Stéphane Quellec, Tiphaine Lucas, Jordane Ossemond, Martine Morzel, Francoise Nau

Food Research International 169 (2023) 112821

Contents lists available at ScienceDirect

Food Research International

journal homepage: www.elsevier.com/locate/foodres

Quantitative magnetic resonance imaging of *in vitro* gastrointestinal digestion of a bread and cheese meal

Maja Musse [a,*], Steven Le Feunteun [b], Guylaine Collewet [a], Mattéi Ravilly [a], Stéphane Quellec [a], Jordane Ossemond [b], Martine Morzel [b], Sylvain Challois [a], Françoise Nau [b], Tiphaine Lucas [a]

[a] *INRAE, OPAALE, 35044 Rennes, France*
[b] *INRAE, Institut Agro, STLO, 35042 Rennes, France*

A B S T R A C T

The monitoring of food degradation during gastrointestinal digestion is essential in understanding food structure impacts on the bioaccessibility and bioavailability of nutrients. Magnetic Resonance Imaging (MRI) has the unique ability to access information on changes in multi-scale structural features of foods in a spatially resolved and non-destructive way. Our objective was to exploit various opportunities offered by MRI for monitoring starch, lipid and protein hydrolysis, as well as food particle breakdown during the semi-dynamic *in vitro* gastrointestinal digestion of complex foods combined in a meal. The meal consisted of French bread, hard cheese and water (drink), with a realistic distribution of bolus particle sizes. The MRI approach was reinforced by parallel chemical analysis of all macronutrients in the supernatant. By combining different imaging protocols, quantitative MRI provided insights into a number of phenomena at the level of the cheese and bread particles and within the liquid phase that are hard to access through conventional approaches. MRI thus revealed the progressive ingress of fluids into the bread crust and the release of the gas trapped in the crumb, the erosion of cheese particles, the creaming of fat, the disappearance of small food particles and changes in liquid phase composition. Excellent agreement was obtained between the quantitative parameters extracted from the MRI images and the results of the chemical analysis, demonstrating the strong potential of MRI for the monitoring of *in vitro* gastrointestinal digestion. The present study proposes further improvements to fully exploit the capabilities of MRI and constitutes an important step towards the extension of quantitative MRI to *in vivo* studies.

1. Introduction

Gastrointestinal digestion is a complex dynamic process during which food structures are broken down into absorbable nutrients. The monitoring of food degradation during the gastric and small intestinal phases of digestion is essential for understanding the mechanisms regulating the bioaccessibility and bioavailability of nutrients. In recent years, this field of research has seen rapid growth and internationally recognized *in vitro* digestion protocols (Brodkorb et al., 2019; Mulet-Cabero et al., 2020) have now been established, making it possible to circumvent the main difficulties associated with *in vivo* experiments (*i.e.*, cost, biological variability and ethical concerns). However, the greater part of these studies have been carried out on single foods, mostly in extensively ground form, and only one macronutrient has been considered. These conditions are not representative of the *in vivo* reality of the ways food is prepared and consumed, consisting in meals made of different food items that contain all macronutrients and are reduced to particles of several millimetres in size during oral breakdown. There is therefore a need to better mimic the complexity of human digestion under controlled *in vitro* conditions in order to link *in vivo* and *in vitro* approaches. The development of non-invasive analytical methods relevant to both approaches is key for the achievement of this last objective.

Magnetic Resonance Imaging (MRI) can be used for spatially resolved measurements of internal micro and macro structures and to provide information on sample composition. This has meant that the benefits of MRI reach beyond the field of medical diagnostics, extending to the food, plant and material sciences and to chemical engineering (Benders and Blümich, 2019; Van As and van Duynhoven, 2013). The MRI signal of protons is mainly defined by NMR relaxation (*i.e.*, longitudinal (T_1) and transverse (T_2) relaxation parameters, proton density and resonance frequency) and the self-diffusional parameters of water and lipids. With the appropriate MRI pulse sequences, acquisition parameters and image processing methods, MRI can be used to quantify the relaxation times that provide information on the molecular environment and diffusivity of water at short distances, giving insights into fluid composition (changes in the concentration and structure of macromolecules) and confinement. MRI can also be used to quantify morphological characteristics, fat/water/air fractions and self-diffusion coefficients. A number of such applications of MRI are in use for the characterization of food products and processes (Mariette et al., 2012). MRI is thus a highly promising approach to overcome the challenges in

* Corresponding author.

https://doi.org/10.1016/j.foodres.2023.112821
Received 14 December 2022; Received in revised form 27 February 2023; Accepted 11 April 2023
Available online 14 April 2023

the monitoring of digestion cited above.

To date, most MRI studies on food digestion have been performed *in vivo* (Smeets, Deng, van Eijnatten, & Mayar, 2021). These studies were mostly confined to the monitoring of large-scale phenomena such as the kinetics of gastric emptying or the visual appearance of gastric content (Freitas, Souchon, & Le Feunteun, 2022; Hornby et al., 2021). The main reason for this limited scope is the compromise that must made between time and space resolutions and image quality to prevent the appearance of artefacts caused by movement (respiratory, gastrointestinal, etc.). As a consequence, the potential of MRI as a technique to monitor the degradation of foods (transfers and hydrolysis) has been largely neglected thus far. Here, the *in vitro* MRI approach (Deng et al., 2022, 2020; Mayar et al., 2022) comes into its own, offering favourable conditions for signal interpretation in relation to chemical and structural changes, while allowing rapid, but quantitative acquisition sequences to be dimensioned using this upstream knowledge. This route has been explored in very recent studies (Deng et al., 2022,2020) by monitoring the *in vitro* digestion of protein gels and evaluating relaxation times in order to predict protein concentration and pH changes in digesta.

The aim of the present study was to evaluate the use of MRI in the monitoring of starch, lipid and protein hydrolysis associated with food breakdown during the semi-dynamic *in vitro* digestion of a complex meal comprised of French bread (crumb and crust), hard cheese and water. The meal was selected to ensure the inclusion of all macronutrients, i. e. carbohydrates, proteins and lipids, with particular characteristics: the main component of the bread samples was starch, with only a small proportion (<10%) of proteins, while the cheese contained a high proportion of proteins and lipids. Additionally, the two foods have rather hard texture (French bread has a hard, brittle crust), meaning that their oral breakdown produced large particles of typically 0–5 mm in size (Jalabert-Malbos et al., 2007). These relatively large sizes make it possible to analyse the structural and physicochemical evolution of realistic bolus particles during the digestion of different foods combined in the same meal. MRI protocols, which to our knowledge have not previously been used in the field of food digestion, were developed to monitor the morphological evolution of solid food particles and to quantify lipids for the characterization of fat creaming. The dynamic evolution of the relaxation times in the different solid and liquid fractions of the digesta was also evaluated to obtain information on hydrolysis kinetics and/or pH variations. All MRI results were compared to conventional chemical analyses.

2. Materials & methods

2.1. Materials

2.1.1. Foods

Commercial cheese and bread were used. The hard cheese was an Emmental (Emmental français, Cora, France), bought in a local supermarket, containing 28% lipids, 28% proteins and 1% carbohydrates (w/w). The bread was made of whole-wheat flour, bought as frozen part-baked sliced loaves (Pain complet tranché, Picard, France) in a local supermarket. Before each experiment, the baking process was completed by defrosting 450 g bread loaves, heating them at 210 °C for 40 min, and leaving them to cool for 30 min at room temperature. The water content of the resulting bread crumb and crust was about 40% (w/w) with a macronutrient composition of 1.7% lipids, 8.1% proteins and 41.8% total carbohydrates (including 3.0% sugars).

2.1.2. Digestive enzymes and inhibitors

Frozen pooled human saliva was obtained from Lee Biosolutions (ref. 991–05-P, Maryland Heights, United States). Porcine pepsin (P6887), porcine pancreatin (P7545), bovine bile extract (B3883), and the enzyme inhibitors Pepstatin A (P5318), Pefabloc (76307), and 4-Bromophenylboronic acid (B75956) were all obtained from Sigma-Aldrich (France). Enzyme activity and bile salt concentrations were determined according to the protocols described in (Minekus et al., 2014).

2.1.3. Other materials

Amyloglucosidase from *Aspergillus Niger* (ref. 10102857001) was obtained from Sigma-Aldrich (France). D-Glucose kits (ref. 10) were obtained from BioSenTec (Portet-sur-Garonne, France). The water was Milli-Q water, the UV–Vis microplate reader was a Multiskan™ GO microplate spectrophotometer (Thermo Fisher Scientific, Waltham, MA, USA), and all other materials were of standard analytical grade.

2.2. Semi-dynamic gastro-intestinal in vitro digestion

The digested meal consisted of 4 g of bread, 4 g of cheese and 8 mL of water (as a drink). Two series of digestion experiments were performed in triplicate using the same protocol: one to monitor the digestion process via MRI (referred to below as “MRI experiments”), and another (non-MRI) to monitor pH evolution and the kinetics of enzymatic hydrolysis via the chemical analysis of collected samples (referred to below as “biochemical experiments”). The digestion procedure was based on the semi-dynamic *in vitro* digestion protocol devised by the INFOGEST consortium (Mulet-Cabero et al., 2020), with two sets of adaptations. First and as described below, we performed a simulation of the oral phase that corresponded more closely to physiological processes by introducing realistic distributions of food particle sizes in the *in vitro* boluses, and by using pooled human saliva rather than a simulated salivary fluid. Second, as a compromise between the digestion protocol recommendations and the constraints associated with MRI measurements, gradual gastric emptying was not considered in our experiments and a stepwise procedure was used for both mixing and the gradual addition of gastric fluid. All other experimental conditions were in compliance with the INFOGEST semi-dynamic *in vitro* digestion protocol.

2.2.1. Experimental setup

A double-wall 90 mL glass vessel with truncated cone (Ref 61418220, Metrohm) was maintained at 37 °C by circulating water. For the MRI experiments, the water-bath was located outside the Faraday cage, and a lid was used to prevent water evaporation. For the biochemical experiments, a lid with apertures was used to monitor the pH using a titration unit (Ref 28420010, 842 Titrando, Metrohm) and to collect samples. About 20 min before the start of the digestion experiments, 1.8 mL of simulated gastric fluid (SGF) at pH 2.0 and 8 mL of water (to represent the drink included in the meal) were added to the vessel and left to warm. Just before the start of the experiments, 0.2 mL of a pepsin solution (40,000 U/mL), prepared freshly and kept on ice, was also added.

2.2.2. Oral phase

2.2.2.1. Food comminution. Both the crumb and the crust of the freshly re-baked bread were used. They were separated by using a knife to cut the crusty bottom flat edge (thickness ~ 3.5 mm) from two slices taken from the middle of the loaf. The crumb was ground using a blender for 5 s at speed setting 2 (8010S, Waring Laboratory Science) to simulate comminution. This procedure was selected because it has previously been reported to provide a suitable simulation of the textural and digestive properties of *in vivo* bread crumb boluses (Freitas, Le Feunteun, Panouillé, & Souchon, 2018). The literature on food oral processing lacks data on the size of crust particles in French bread boluses. It has, however, been found that, in French baguettes, the median equivalent diameter of bolus particles increased from 3.0 mm (crumb only) to 4.1 mm where crust was present, with an increased heterogeneity in distribution (Jourdren et al., 2016). Assuming that this effect can be attributed to crust particles that are larger than crumb particles, crust

comminution was simulated by using a knife to produce parallelepipeds of approximated size: 5 mm × 5 mm × 3.5 mm. This choice was also a practical one for the present study, in that it allowed the monitoring of these particles by MRI. Crust and crumb samples were then combined in a ratio of 30:70 (1.2 g/2.8 g) to maintain the crust/crumb ratio of the original bread, and were stored in a closed laboratory container until the saliva was added.

Cheese comminution was performed by grinding large cheese pieces for 2 periods of 10 s at speed setting 2 (same blender) and by passing the resultant particles through a sequence of sieves with decreasing mesh sizes (4, 2, and 1 mm). Additionally, larger cheese cubes with sides of approximately 5 mm were produced using a knife. Cheese particles from the 4 fractions (<1 mm, 1–2 mm, 2–4 mm, and 5 mm cubes) were then combined in the following proportions respectively: 10:40:30:20 (0.4 g/1.6 g/1.2 g/0.8 g), to reproduce the particle size distribution reported for Emmental boluses in humans (Jalabert-Malbos et al., 2007). The cheese particles were stored at −25 °C and defrosted on the day of the digestion experiment.

2.2.2.2. Imbibition by saliva. To begin the digestion experiment (t = 0 s), 4 g of bread particles were combined with 4 g of cheese particles to which 4 mL of human saliva had been added and mixed for 30 s with a spatula. At t = 90 s, the *in vitro* bolus was transferred to the digestion vessel and mixed for 30 s with a spatula. The end of the oral phase and the start of the gastric phase were considered to occur at t = 2 min.

2.2.3. Gastric phase

In the MRI experiments, the pH of the supernatant was measured at t = 2 min at the entrance to the Faraday cage, the vessel was rapidly positioned within the MRI device, and a first block of MRI acquisitions was performed. In the biochemical experiments, the pH electrode of the titration unit was immersed within the vessel and pH recording was initiated.

In both the MRI and biochemical experiments, the addition of gastric secretions and mixing were performed using a stepwise procedure consisting in five additions of 3.24 mL of simulated gastric acid (0.25 M HCl) and 360 μL of simulated pepsin solution (gastric lipase was not used), followed by 20 s of mixing (spatula). Intervals of approximately 18 min (time between two sets of MRI acquisitions) were observed between consecutive additions. As illustrated in Fig. 1A, this procedure allowed pH ∼ 2 to be reached and the addition of SGF (final pepsin activity of 2,000 U/mL in a volume of 40 mL) to be completed at about t = 92 min. A last mixing step of 20 s, with no prior addition of SGF, was performed 18 min later (t = 110 min), and the gastric phase was pursued for a further 20 min (until t = 130 min).

At the end of the gastric phase, the pH was measured (at the entrance to the Faraday cage in the MRI experiments), raised to pH ∼ 7 with NaOH 4 M, and 4 mL of samples were collected from the supernatant and stored at −25 °C to await further analysis. During the biochemical experiments, additional samples of 1 mL (to which 50 μL of pepstatin A at 0.5 mg/mL in methanol had been aded), 0.6 mL (without stabilisation because gastric lipase was not used), and 1 mL (heat treated at 99 °C for 5 min) were collected from the supernatant at t = 5, 27, 47, 92 min, and stored at −25 °C to await assessment of the release kinetics of the products of protein, lipid and starch hydrolysis, respectively.

2.2.4. Intestinal phase

After the sampling at the end of the gastric phase, 28.8 mL of 1.25 × concentrated simulated intestinal electrolyte solution and 2 mL of bile solution (final concentration of 10 mM of bile salts) were added, the pH was adjusted to 7.5 using NaOH 4 M, and water was added to bring the vessel volume to 68 mL. It should be noted that the pH was adjusted to 7.5 to try to obtain a mean pH that would remain close to 7.0 during the intestinal phase, as recommended in the INFOGEST protocol (Mulet-Cabero et al., 2020). As illustrated in Fig. 1A, this is because pH

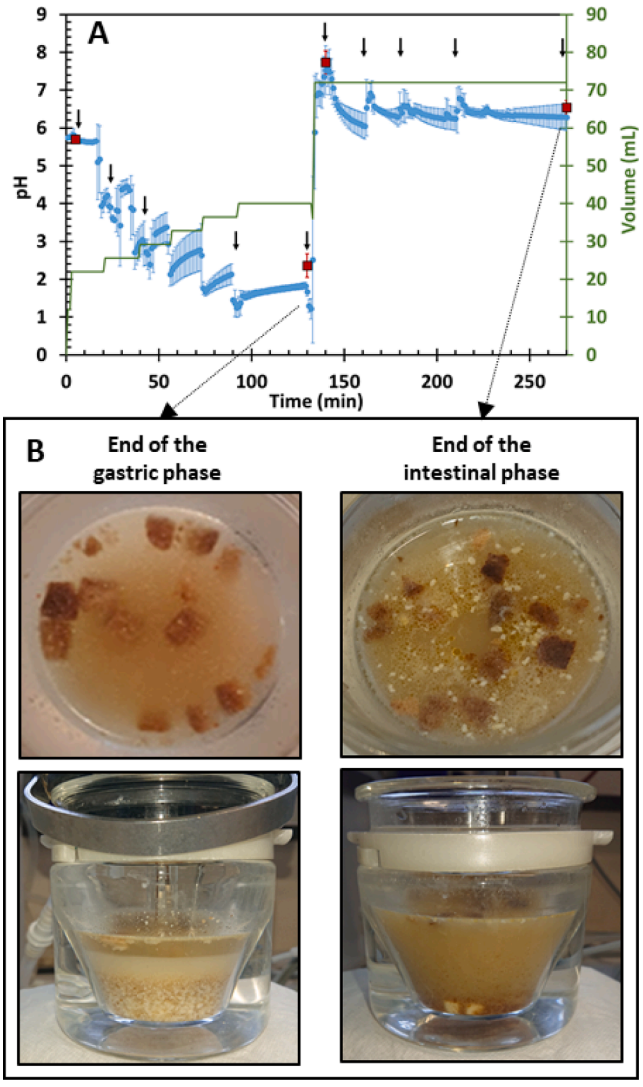

Fig. 1. (A) Overview of the experimental conditions during the digestion experiments. Blue circles and red squares represent pH evolution during the biochemical and MRI experiments (left-hand y-axis), respectively. Values are mean ± standard deviation for 3 replicates. The solid green line represents the time-course of the digesta volume during the MRI experiments (right-hand y-axis), and arrows indicate the times at which samples were collected from the supernatant during the biochemical experiments. (B) Visual appearance of the digesta at the end of the gastric and intestinal phases. (For interpretation of the references to colour in this figure legend, the reader is referred to the web version of this article.)

continuously decreases during the small intestinal phase due to the progressive release during the intestinal phase of protons previously entrapped by food particles during the gastric phase. The intestinal phase was then launched (after returning the vessel to the MRI device for the imaging experiments) by adding 4 mL of pancreatin (final trypsin activity of 100 U/mL in a volume of 72 mL) and mixing for 20 s with a spatula.

As previously for the gastric phase, mixing was performed using a stepwise procedure consisting in 20 s of mixing with a spatula at intervals of approximately 18 min corresponding to time between two sets of MRI acquisitions. At the end of both the MRI and biochemical experiments (t = 270 min), pH was measured, and 4 mL of samples were collected and stored at −25 °C. In the course of the biochemical experiments, additional samples (1 mL to which 50 μL of Pefabloc 0.1 M was added, 1 mL to which 50 μL of boronic acid 0.1 M was added, and 1 mL heat-treated at 99 °C for 5 min) were collected from the supernatant

at t = 140, 160, 170, 210 min, and stored at −25 °C for use in further assessment of the release kinetics of nutrients. The digestion mixtures left over from the biochemical experiments were also stored at −25 °C and were used to estimate the final quantity of creamed lipids.

2.2.5. Creaming of lipids

The mass of creamed lipids at the end of the intestinal phase of the biochemical experiments was evaluated using the following procedure. The digestion mixture was thawed then centrifuged (5000*g* for 20 min at 4 °C), and the pellet was discarded. The retained fraction, comprising an aqueous phase, a creamed layer and small floating cheese particles (Fig. 1B), was weighed before being homogenized with a ultra-turrax (IKA-T25 with the axis S18N-10G/03.444838; 25,000 rpm). A 1 mL sample was then collected and stored at −25 °C to await analysis of its lipid content.

Complementary experiments were performed to estimate the rate and extent of lipid creaming during the early stages of the gastric phase, as this phenomenon was visually noticeable. Three experiments were launched in duplicate using the same protocol as that employed in the biochemical experiments, and were stopped after 5, 25 and 45 min of gastric digestion. The digestion mixture was immediately centrifuged (same conditions), the pellet was discarded, and the remaining fraction was collected and weighed. In these gastric samples, the small floating cheese particles tended to remain stuck to each other during attempts to homogenize them using the ultra-turrax. An intestinal digestion protocol was therefore applied to these samples before they were homogenized with the ultra-turrax and the 1 mL samples were collected for storage at −25 °C to await analysis of their lipid content.

2.3. MRI acquisition

MRI measurements were carried out on a 1.5 T MRI scanner (Magnetom, Avanto, Siemens, Erlangen, Germany) with a 4-element head-array receiver coil. Four series of MRI images were acquired using following protocols:

(1) A 2D multi spin echo (MSE) sequence to estimate T_2 maps for the central vertical section of the digestion reaction vessel's contents.
(2) A 2D MSE sequence to estimate T_2 maps for the uppermost horizontal section of the vessel's contents, located immediately below the surface.

This 2D MSE sequence (Adriaensen et al., 2013) was performed with a non-selective refocusing pulse, making it possible to shorten echo time (TE) for sampling the relaxation curves of the bread and cheese samples, which were characterized by relatively low T_2 values. Parameters were set at TE 5.4 ms, repetition time (TR) 868 ms, 82 echoes per echo train, bandwidth 383 Hz/pixel, 1 scan, field of view (FOV) 280 × 280 mm^2, 5.1 mm slice thickness and a 192 × 192 pixel matrix. Acquisition time for each image series was 2 min 46 s and in-plane image resolution was 1.5 × 1.5 mm^2.

(3) A 3D ultra-short echo time (UTE) sequence to quantify the volume of large cheese particles with TE 70 μs, TR 5 ms, flip angle 15°, FOV 93 × 93 × 93 mm^3, number of projections 10,000, matrix size 128x128x128, bandwidth 399 Hz/pixel, 4 scans. Acquisition time was 2 min 46 s and image resolution was 0.73 × 0.73 × 0.73 mm^3.
(4) A 3D gradient echo (GRE) sequence used to quantify the fat fraction using the water-fat separation approach as described in (Hernando et al., 2010). Parameters were set at first TE 1.48 ms, echo spacing 2.81 ms, 6 echoes per echo train, TR 50 ms, flip angle 15° making it possible to reduce T_1-weighting, FOV 128 × 128 × 64 mm^3, matrix size 128 × 128 × 64, bandwidth 888 Hz/pixel, 1 scan. Acquisition time was 6 min 51 s and image resolution was 1 × 1 × 1 mm^3.

TR was chosen in a preliminary study as a compromise between the acceptable signal to noise ratio (SNR) and the acquisition time related to the digestion kinetics. In the case of MSE sequence, the number of echoes needed to sample relaxation decay was also considered. The imaging sequences were launched in the above order. Note that the circulation of the temperature-controlled fluid was interrupted during the acquisition of both the MSE sequence for the horizontal T_2 mapping of the vessel's contents and the 3D GRE images, to prevent artefacts from appearing in the images.

2.4. Image processing

2.4.1. Segmentation of large cheese particles from UTE images

The cheese was semi-manually delineated in the UTE images using Avizo 3D Pro software (FEI Company, version 2021.2). No attempt was made to delimit each particle separately because, aside from the complexity of the task itself, such an exercise would have been pointless given that the mixing of the contents of the vessel between each acquisition would have precluded the tracking of individual particles.

2.4.2. T_2 Maps

Mono-exponential T_2 maps of the vertical and horizontal sections were computed using Scilab software from the images acquired with the MSE sequence by fitting the relaxation curves using the Levenberg-Marquardt algorithm. Only echoes characterized by SNR greater than 7 were used, making it possible to assume a zero-mean Gaussian noise distribution in the magnitude images. Mean T_2 values were computed at the scale of the regions of interest (ROI) for the different phases and food particles, as described below.

Voxel with T_2 values lower than 135 ms were considered as corresponding to bread crust. This thresholding value was chosen by visual observations. The segmentation was applied until the image acquired at 160 min, from which the thresholding became less relevant.

2.4.3. Lipid quantification

Separation of water and lipid signals was carried out using the 3D GRE images and the method detailed in (Picaud et al., 2016). This method is based on the difference in signal frequency between the hydrogen protons of water molecules and those of lipid molecules. The correction of B_0 field inhomogeneities is included in the method thanks to the acquisition of images at multiple TE. The method requires an *a priori* knowledge of the composition of the lipid. We used the data provided in (https://www.agroscope.admin.ch/agroscope/fr/home/themes/denrees-alimentaires/alimentation-sante/lait-produits-laitiers/graisse-du-lait.html), taking these to represent the average lipid composition of dairy fat. We obtained images of the quantity of lipids, referred to hereafter as "lipid maps". 3D Data were represented in 2D as the sum of the lipid maps over the horizontal direction. A complementary experiment using a known quantity of lipids made it possible to convert the MRI lipid signal into grams. The sum of the lipid mass present in the bottom 1.5 cm of the glass vessel holding the cheese particles under observation was used as a quantitative indicator of fat creaming.

2.5. Sample analysis

All the samples collected from the supernatant were thawed (16 h, 4 °C) and centrifuged (10,000*g* for 20 min at 4 °C). Three phases were obtained: a lipid phase at the top, a pellet, and a large intermediate aqueous phase containing water-soluble compounds and lipolysis products solubilized in bile salts (intestinal phase). Five hundred μL of the aqueous intermediate phase were collected and stored at −25 °C to await assessment of the release kinetics of starch, protein and lipid hydrolysis products into the supernatant.

2.5.1. Released starch

The release of water soluble starch fractions, dextrins and maltose

(referred to as "released starch" for the sake of simplicity) was quantified as glucose equivalent (D-glucose kits) following complete hydrolysis with amyloglucosidase using a previously described protocol (Freitas, Le Feunteun, Panouillé, & Souchon, 2018) adapted to microplates. The results were converted into starch equivalent concentrations (g/L) using a conversion factor of × 0.9 (Goñi et al., 1997).

2.5.2. Released proteins

The release of free primary amino groups (NH_2) in the supernatant, which is indicative of the release of proteins, peptides and amino-acids, was measured using a previously described o-phthalaldehyde (OPA) spectrophotometric assay in microplates (Salelles et al., 2021). Results were corrected for digestive secretions (blanks with no food), and converted into free NH_2 concentrations (mM) using a calibration curve created with L-methionine (0–2 mM). As these results cannot be directly converted into protein hydrolysis product masses, complementary analyses were performed using the Kjeldahl method (N × 6.38) to estimate the true content of the end samples of both the MRI and biochemical experiments (correcting the protein content of the digestive secretions).

2.5.3. Solubilized and creamed lipids

The release of fatty acids and monoacylglycerols in the supernatant (referred to as "solubilized lipids") was quantified as "total fatty acid" (TFA) using a gas chromatograph mass spectrometer (Shimadzu GCMS QP2010 SE equipped with a BPX70 capillary column: 120 m, 0.25 mm i.d., 0.25 μm film; SGE Analytical Science, Australia) after transmethylation of the samples (according to an internal C13 standard), and hexane extraction using the procedure previously described in (de Figueiredo et al., 2021). The same procedure was used to quantify the total lipids contained in the upper phases of the centrifuged digestion

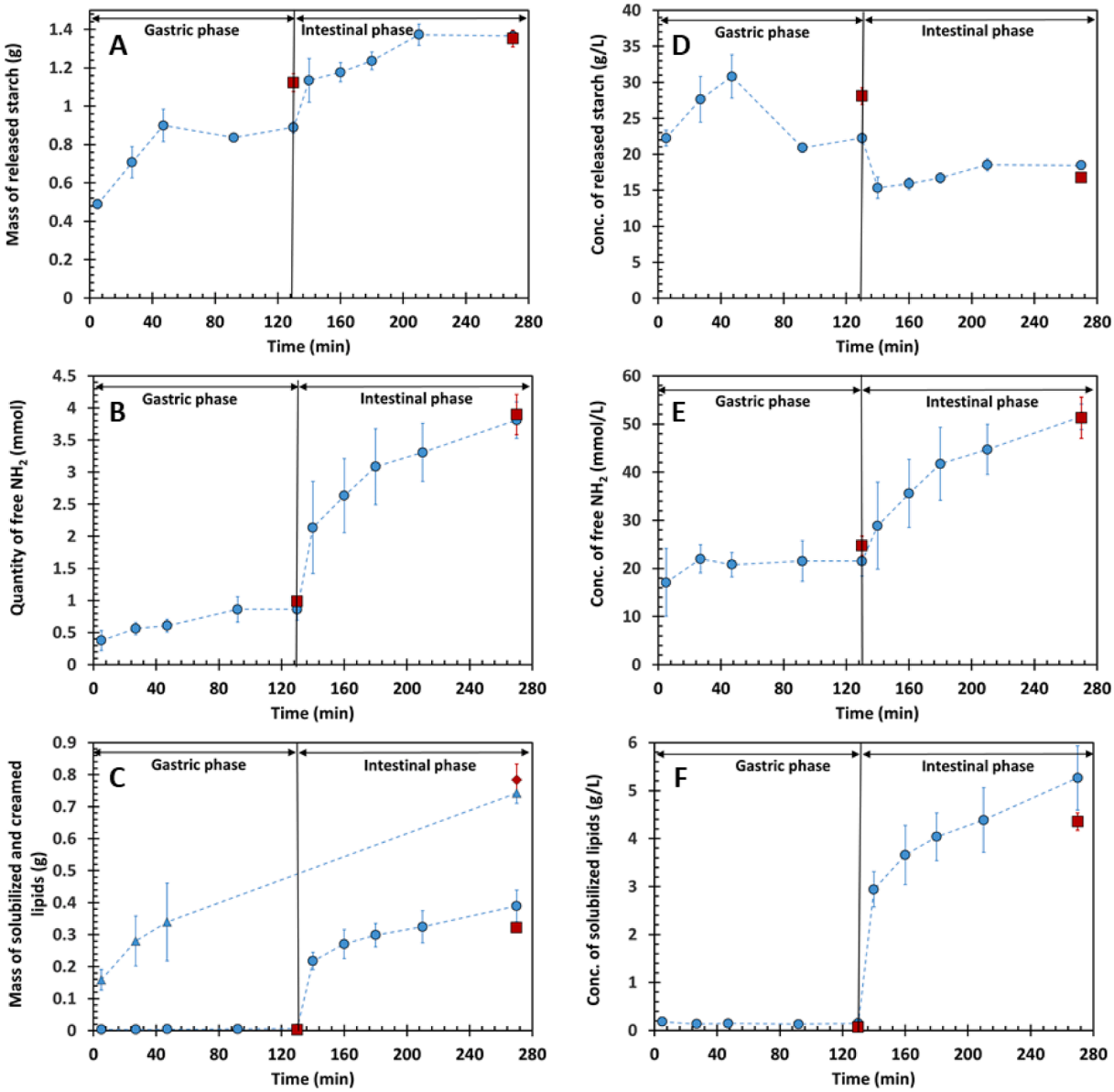

Fig. 2. Release kinetics of starch, free NH_2 and lipid products in the supernatant during digestion. Subplots (A), (B) and (C) show the cumulative masses or quantities of released starch, free NH_2 and solubilized and creamed lipids, respectively, while subplots (D), (E) and (F) show their respective concentrations in the supernatant (creamed lipids excepted). Blue circles and red squares denote the biochemical and MRI experiments, respectively. The blue triangles and red diamonds in subplot (C) denote the results obtained for both creamed and solubilized lipids (samples collected during complementary experiments for the gastric results). Values are mean ± standard deviation for 3 replicates except in the gastric results for creamed and solubilized lipids (2 replicates). (For interpretation of the references to colour in this figure legend, the reader is referred to the web version of this article.)

mixtures during the early stages of the gastric phase and at the end of the intestinal phase of both the biochemical and MRI experiments.

2.5.4. Data correction

The volume of the samples collected during the biochemical experiments and their released nutrient content must be taken into account. To correct for the effects of these on the concentrations measured and enable a fair comparison between the biochemical and MRI experiments, the cumulative contents of released starch, free NH_2, and solubilized lipid products were calculated, taking into account the materials removed. The corrected concentrations were then computed by dividing the cumulative nutrient contents (g or mmol) by the reaction volume that would have been present without sampling in the course of the gastric and intestinal phases (as in the MRI experiments). In the following, all concentrations and quantities have been corrected for the effects of sample removal.

3. Results

3.1. Chemical analysis of supernatant samples

Fig. 2 shows the release kinetics of starch, free NH_2, and lipid compounds, respectively, in the supernatant of the centrifuged samples. Fig. 2A shows the mass of released starch during digestion, regardless of its level of enzymatic degradation. The starch kinetics displayed an exponential-like increase during both the oro-gastric and small intestinal phases. The mass of the released starch increased to about 0.5 g within just 5 min of the start of the oral phase. It continued to increase until t = 47 min, and then remained stable until the end of the gastric phase, at around 1.0 g (0.9 g and 1.1 g in the biochemical and MRI experiments, respectively), corresponding to about 58% of the total carbohydrate content (1.71 g) of the meal. Immediately after the start of the intestinal phase, the release of starch resumed until it reached a final plateau at around 1.37 g, corresponding to about 80% of the total carbohydrate content of the meal. These results indicate that the hydrolysis of the starch by salivary α-amylase was initiated from the start of the oral phase and continued until gastric pH reached 3.0 (Fig. 1A), the threshold below which salivary α-amylase is irreversibly deactivated (Freitas and Feunteun, 2019; Fried et al., 1987). The contributions made by the gastric and intestinal phases to the overall release of starch are also consistent with a number of previous reports on various breads (Freitas et al., 2018; Freitas et al., 2022).

Fig. 2B shows the cumulative quantity of free NH_2 measured in the supernatant, which is indicative of the release kinetics of proteins, peptides and amino acids. The gastric and intestinal consecutive increases in free NH_2, which followed a trend similar to that of the starch release kinetics, reached about 0.9 mmol at the end of the gastric phase, and about 3.8 mmol at the end of the experiments. It is of note that the quantity of released NH_2 should slightly underestimate the true contribution of the gastric phase to the overall release of peptides into the supernatant. This is because the extent of protein hydrolysis produced by pepsin action is typically one order of magnitude lower than during the intestinal phase (Mat et al., 2020), leading to the presence of longer peptides and fewer N-terminal ends (free NH_2) for a given mass. According to the results obtained in a parallel study on the same cheese with the same initial particle size distribution (Morzel, Ramsamy, & Le Feunteun, 2023), we may expect the true mass of released peptides during the gastric phase to be about 0.5 g, which would correspond to 34% of the protein content (1.45 g) of the meal. Additionally, complementary analyses carried out on the end samples using the Kjeldahl method showed that a mean protein equivalent mass of about 1.10 g was present in the supernatant at the end of both the MRI and biochemical experiments, corresponding to about 75% of the total protein content of the meal. These estimated contributions of the gastric (34%) and intestinal phases (75%) to the release of proteins are of the same order of magnitude as previous findings on cheese digestion *in vitro*, where values in the ranges of about 40–50% and 50–70% have been reported for different cheeses at the end of the gastric and intestinal phases (with a 1 h-long intestinal phase), respectively (Fang et al., 2016).

Fig. 2C shows the cumulative mass of the lipids solubilized into the supernatant during the experiment, as well as the overall mass of released lipids (solubilized and creamed) at the four digestion time points investigated. Because lipids are not water soluble, only traces of solubilized lipids were measured during the gastric phase. However, significant quantities of creamed lipids were measured in the early stages of the gastric phase. At t = 5, 27 and 47 min, means of 0.16, 0.28 and 0.34 g of total fatty acids (TFA) were recovered from the creamed layer, representing about 15, 27 and 32% of total lipid content (1.05 g of TFA), respectively. During the intestinal phase, a rise in solubilized lipids was observed, due to the presence of bile salts, which can solubilise the free fatty acids and monoacylglycerols produced during lipolysis. The observed kinetics was in line with what is classically observed in *in vitro* digestion studies, displaying a rapid initial reaction rate that tends to decrease progressively (Mat et al., 2020). The quantity of lipolysis products solubilized in the aqueous phase of the supernatant was about 0.22 g just after the start of the intestinal phase and reached about 0.39 g at the end of the biochemical experiments (0.30 g in the MRI experiments), corresponding to 37% of the TFA content of the meal. When creamed lipids were also included, the total amount of TFA recovered in the supernatant at the end of the biochemical experiments was 0.74 g (0.78 g in the MRI experiments), corresponding to about 70% of the initial TFA content of the meal. This recovery percentage was in fair agreement with that obtained for proteins (~75%), given that most of the protein and lipid contents of the meal were known to come from the cheese. At the end of the experiments, about half (53%) of the lipids recovered in the supernatant were, therefore, in the form of lipolysis products solubilized in bile salts, while the other half were found in the creamed layer.

Fig. 2D, E and F show the concentration profiles of the released starch, free NH_2 and solubilized lipids, respectively, since parametric measurements by MRI is sensitive to concentration. For all nutrients, the trends observed during the intestinal phase were identical to those previously described for the cumulative contents because the reaction volume was constant as the result of the data correction for sample removal. During the gastric phase, however, concentration profiles depended on the balance between the release of nutrients into the supernatant and the dilution induced by the stepwise addition of gastric secretions. This dilution factor increased by 16.5%, 33% and 82% respectively between the first sampling time (t = 5 min) and the next three (at t = 27 min, 47 min and 92 min). As shown in Fig. 2B, nutrient release and dilution combined led to a three-stage concentration profile for released starch during the gastric phase – a rapid increase up to t = 47 min (*i.e.* until the end of the starch release kinetics, Fig. 2A), a decrease upon dilution preceding the 92 min time point, and a plateau. The concentration profile of free NH_2 was very stable throughout the gastric phase (Fig. 2E), thereby indicating that the release of proteins and peptides was counterbalanced by the increasing dilution. As previously explained, only trace concentrations were measured for solubilized lipids (Fig. 2F) because of their very low water solubility.

3.2. T_2 Maps of the digesta

Fig. 3A shows a typical set of vertical T_2 maps of the vessel contents during digestion and Fig. 3D shows a typical set of horizontal T_2 maps for the surface of the digesta. A total of four fractions could be distinguished from t ~ 50 min, *i.e.* once the volume of gastric fluid was in excess: an aqueous supernatant, a deposit of cheese and bread crumb particles, the largest cheese particles within the deposit, and the floating bread crust particles. Because these fractions could not be clearly distinguished before t ~ 50 min, Fig. 4A shows the mean T_2 of each phase from that time. Reproducibility between runs was reasonably good for all fractions (Fig. 4A), while the T_2 values between fractions did

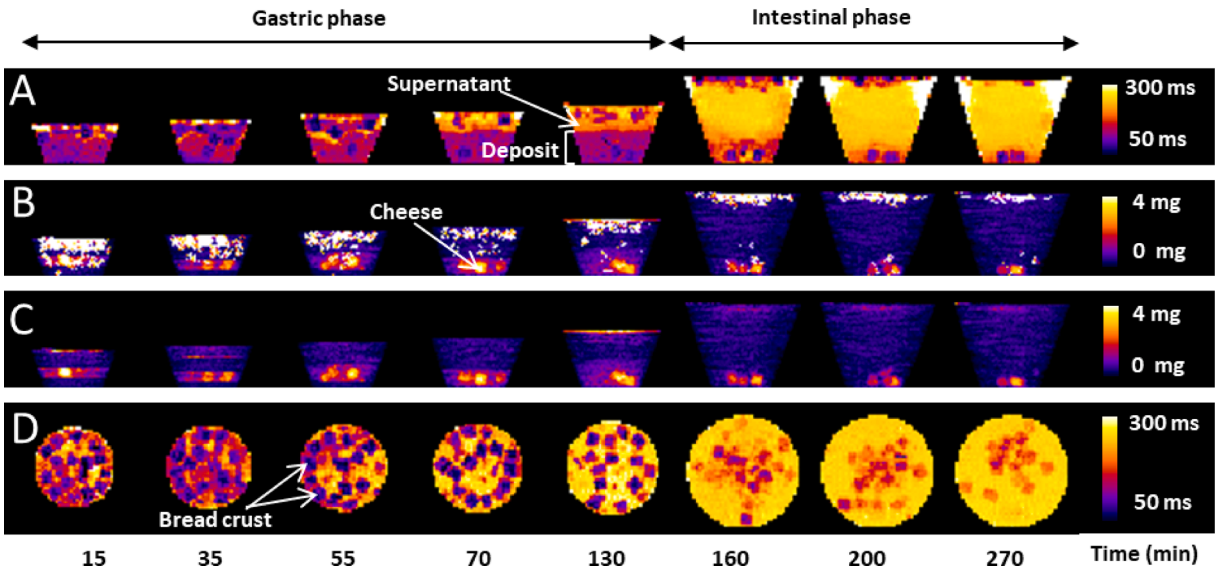

Fig. 3. Representative images of the evolution of the digesta over time according to: (A) the vertical 2D T_2 maps, (B) the sum of the horizontal 3D lipid maps, (C) same as (B) but excluding outlier measurements, and (D) the horizontal 2D T_2 maps located immediately below the surface of the digesta.

not overlap.

Due to their density of nearly 1.1 (Iezzi et al., 2013), the cheese particles tended to collect in the very bottom of the vessel following sedimentation. Some of the largest particles of cheese with sides of ~5 mm were captured in the vertical images. They were recognisable by their cubic section (Fig. 3A) and were found at the same location in the MRI fat maps of the vessel (Fig. 3B), which confirms the assignment of these objects to the cheese. T_2s for the large cheese particles (Fig. 4A), resulting from the relaxation of both water (affected by exchangeable protons in the macromolecules) and fat protons (Chen et al., 2020) increased slightly from about 90 ms at 50 min to about 115 ms.

As expected, bread crumb fragments could be visually observed in the deposit, mostly in the upper part thereof (Fig. 1B). Imbibition occurs rapidly in bread crumb (Mathieu et al., 2016), which swells as a consequence, explaining why crumb fragments accounted for most of the deposit volume. The T_2 values for the deposit plotted in Fig. 4A were, therefore, mostly governed by the T_2 of the bread crumb. The imbibition of the gastric fluid offers a comprehensive explanation for the passage of the crumb T_2 from 12 ms before digestion to ~125 ms at the first measurement point for the crumb within the deposit (at ~50 min). Because of this high rate of imbibition, T_2 of the deposit followed the same pattern as those for the supernatant (Fig. 4A), but with lower values due to the lower dilution and therefore stronger interactions between the water protons and the macromolecules from crumb. Indeed, T_2 values for the deposit and the supernatant (Fig. 4A) did not vary significantly during the period analysed, except at the point of shift between the gastric and intestinal phases, whereas the deposit's volume underwent a rapid and marked decrease (Fig. 4B).

For the uppermost section of the supernatant, the horizontal T_2 maps (Fig. 3D) enabled a better T_2 characterization of the floating crust particles than could also be mapped in vertical section. Close examination showed that T_2 was higher in the periphery than in the core of crust particles; this is illustrated by typical T_2 profiles in Fig. 5. Fig. 4B plots the surface area occupied by the crust core when thresholding at an arbitrary value of T_2 of 135 ms corresponding to a hydration level intermediate between those of the original crust and the supernatant (Fig. 5). This surface area clearly decreased during the gastric phase, thereby evidencing the progressive absorption of the gastric fluid by the crust particles.

3.3. Morphological 3D images of large cheese particles

3D UTE images, with 0.73^3 mm^3 spatial resolution, were used to monitor changes in the volume of the largest cheese particles (Fig. 6). This analysis was not possible during the early gastric phase, as the contrast in UTE images was not sufficient to unambiguously distinguish the cheese and crust particles in the deposit. Fig. 6 shows an example of the 3D MRI images of the cheese particles at the bottom of the vessel, reconstructed from the sequential UTE images. Six to eight particles could be identified at different time points, suggesting that, in addition to the largest cheese particles (about five in number), intermediate-sized cheese fragments, plausibly in the form of agglomerates, could be detected. Fig. 4C presents the evolution of the total volume of these cheese particles segmented from the UTE images. The decrease in cheese volume was generally linear throughout the course of the experiment, resulting in an overall loss at t ~ 50 min of at least half of the first measured volume.

3.4. Lipid maps of the digesta

Fig. 3B presents a typical set of the lipid maps measured during digestion, where the intensity in each voxel is proportional to the quantity of lipids. Each map corresponds to the sum of the 3D volume in the horizontal orientation. The results are obviously wrong in some regions (white voxels), probably due to distortions of the magnetic field device induced by gas bubbles in the bread particles. The frequent appearance of erroneous values for the uppermost section of the digestive fluid, where crust particles floated (Fig. 1B), is consistent with such a hypothesis. For observation purposes, the outlier measurements were excluded from the lipid maps in Fig. 3C. Fig. 3C clearly shows the decrease in cheese volume and the lipid content at the bottom of the vessel over time. From t ~ 50 min, the deposit essentially consisted of cheese and degassed crumb particles, thus making it possible to assess the progressive loss of lipids within the deposit during digestion (Fig. 4D). Within the bottom 1.5 cm of the glass vessel, where all the large cheese particles were observed to have collected, the lipid mass of about 0.5 g estimated at t ~ 50 min appeared to be only half of the initial lipid content of the meal. Such a rapid and acute decrease can only be explained by the occurrence of creaming at the beginning of gastric digestion. During the second part of the gastric phase, MRI measurements showed the quantity of lipids in the deposit to remain roughly constant, before a further quarter of the initial lipid content was lost at

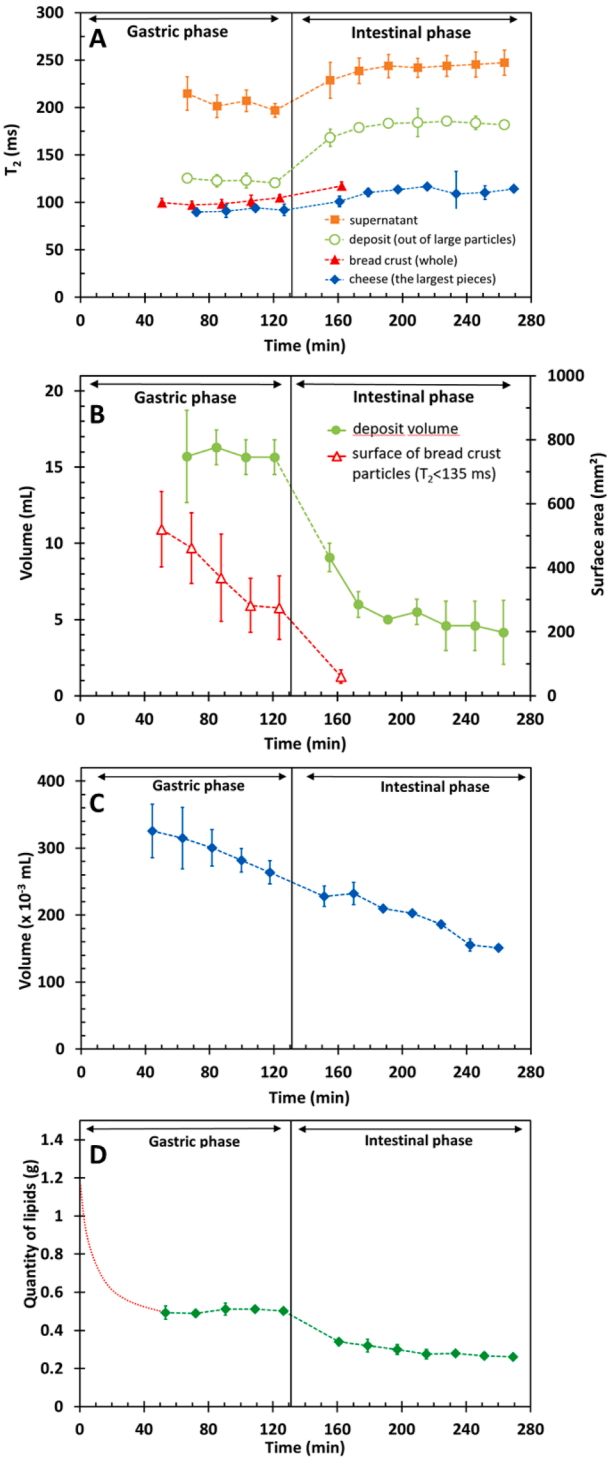

Fig. 4. Evolution of the parameters computed from the MRI images during digestion. (A) T_2 in the different fractions of the digesta (supernatant, deposit out of large particles, bread crust particles and large cheese particles). (B) Volume of the deposit (left-hand y-axis) and core surface (right-hand y-axis) of the bread crust particles as estimated from the 2D T_2 horizontal maps (threshold in Fig. 5). (C) Volume of the large cheese particles as estimated from the 3D UTE images. (D) Lipid mass estimated by 3D GRE images within the lowest 1.5 cm of the glass vessel during digestion. The dotted red line provides a visual guide linking the first MRI measurements at t ~ 50 min with the initial lipid mass contained in the meal. Values are mean ± standard deviation for 3 replicates. (For interpretation of the references to colour in this figure legend, the reader is referred to the web version of this article.)

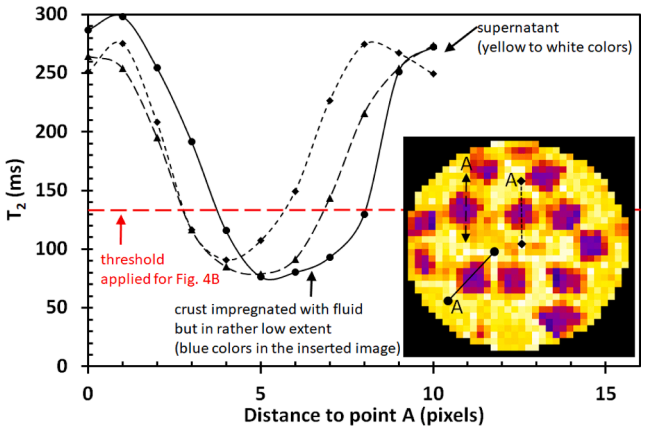

Fig. 5. Example of a T_2 profile across a bread crust particle at the surface of the digesta with superimposition of the threshold used to delimit the hydrated particles in Fig. 4B. Different symbols denote the 3 exemplary profiles.

the very beginning of the intestinal phase. At the end of the experiments, the mass of the lipids in the deposit was estimated to be about 0.25 g.

4. Discussion

The present MRI study allowed investigation of a great variety of phenomena that occur during the semi-dynamic *in vitro* digestion of a bread and cheese meal, namely, the slow ingress of digestive fluid into dry food particles (bread crust), the release of the gas trapped in soft aerated particles (bread crumb), the enzymatic erosion of millimetre-sized solid particles (cheese), the progressive loss of small food particles from the volume of the deposit, and the creaming of cheese fat, along with the NMR parameters (T_2) for food particles and the supernatant that can be related to their physicochemical properties (e.g. microstructure, composition, pH). The quality of these MRI-based findings is discussed in what follows, considering each mechanism in turn.

It should be noted in particular that it is beyond the scope of the present paper to further discuss the chemical analysis results in their own right (Fig. 2), especially in respect of the many enzymatic reactions and physicochemical processes at work. We simply point out that the overall trends obtained from the chemical analyses are in very good agreement with the expected chronology and extent of enzymatic actions (Capuano and Janssen, 2021; Le Feunteun et al., 2021). Readers who wish to discover more about the chemical processes involved in starch, protein, and lipid digestion are invited to refer to the abundant literature available on these topics and may wish to take the paper describing the INFOGEST semi-dynamic protocol (Mulet-Cabero et al., 2020) as their starting point. The results from the chemical analyses will, however, be fully considered as they relate to the MRI results.

4.1. Physicochemical properties of the different fractions of the digesta

It was anticipated that two main MRI measurement types would provide information on the overall release of nutrients into the aqueous fraction of the supernatant: the measurement of T_2 in the different fractions of the digesta (supernatant, deposit, large particles of cheese and bread crust particles) and the decreasing volume of the deposit, also estimated from T_2 maps.

The T_2 values measured in the different fractions (Fig. 3A) remained largely stable during both the gastric and the intestinal phases (Fig. 4A), though the T_2 values, especially that of the supernatant, might have been expected to evolve more with the decreasing gastric pH and/or the changing soluble nutrient content (Leforestier, Mariette, & Musse, 2021; Hills et al., 1991). The only marked changes were observed for the deposit and the supernatant at the point of transition between the gastric

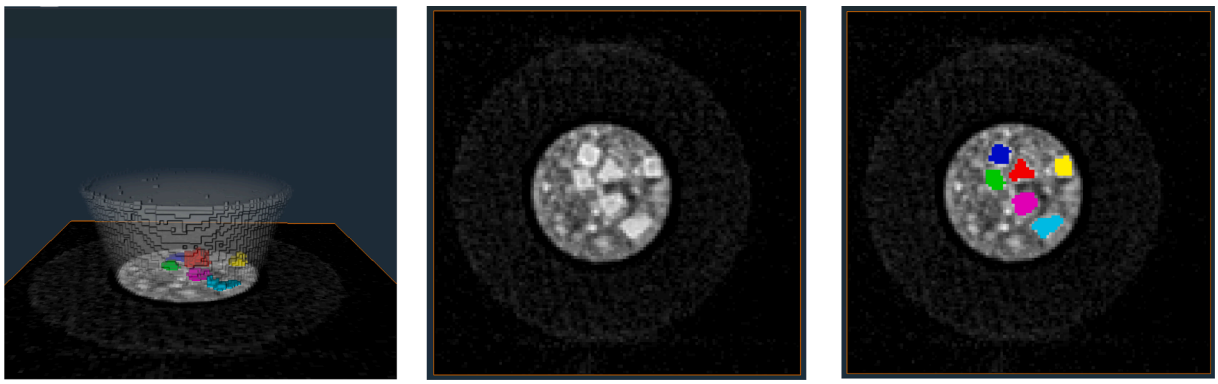

Fig. 6. Examples of 3D views reconstructed from 3D UTE MRI images of the large cheese particles.

and intestinal phases, which can be explained by the sudden rise in both pH and water content following the addition of the intestinal fluid.

A number of explanations are available for the relative stability of the T_2 values during the gastric and intestinal phases of digestion. Of these, the lack of T_2 results for the first ~ 50 min is probably one of the most important. Indeed, by ~ 50 min, the pH was already around 3.0 (Fig. 1A) and the release of starch hydrolysis products, the main nutrient in the gastric supernatant, had already been completed (Fig. 2A), hence leaving no scope for any clear pH- or nutrient-induced T_2 variation. During the intestinal phase, concentration of free NH_2 in the supernatant had more than doubled, but without marked changes in the latter's T_2 values. This could also be considered to contradict the result reported in (Deng et al., 2020) for gastric digestion, but this would be to overlook the far greater complexity of our intestinal supernatant composition, where released peptides not only mix with other hydrolysis products (from starch and lipids) but also with bile and pancreatin compounds. The relative stability of the T_2 values for the largest cheese particles throughout gastric and intestinal digestion (Fig. 4A) can also be explained by the limited diffusion of enzymes, as it is very likely that their protein networks were mostly affected in the peripheral parts only. This would be consistent with the very high buffering capacity of cheese (Salaun et al., 2005; Upreti et al., 2006) and with the previous finding that external erosion is the predominant mechanism for the enzymatic digestion of dairy gels (Floury et al., 2018). Although small, the increasing trend of T_2 in cheese (Fig. 4A) therefore remains compatible with the progressive softening of these particles that could be visually observed during the course of digestion. Similarly, the slow imbibition of liquid by the large crust particles demonstrated by the results shown in Fig. 4B may be associated with the slight but regular increase in their T_2 values.

It is more straightforward to relate the evolution of the deposit volume (Fig. 4B) to the release of nutrients from the particles (Fig. 2). In the earlier stages of the experiment, the bread crumb particles tended to swell, coming to occupy, together with cheese particles, most of the digesta volume (29.2 mL at 50 min). Interestingly, clear separation of the deposit and the supernatant, with a deposit of around 16 mL (Fig. 4B), began immediately after the end of starch hydrolysis by salivary amylase (Fig. 2A). The volume of the deposit then remained roughly constant until the end of the gastric phase, in line with the fact that gastric amylolysis was complete and that the progressive release of free NH_2 (Fig. 2B) was very slow. The quasi-exponential decrease of the deposit volume during the intestinal phase was also in excellent agreement with the release kinetics of NH_2, solubilized lipids, and the remaining starch (Fig. 2). At the end of digestion, the volume of the deposit ranged from 2 to 6 mL, thus representing a ~75% decrease that was compatible with both our visual observations (Fig. 1B) and the 70–80% concentration of nutrients in the supernatant (Fig. 2). Although the decrease in deposit volume allowed no direct identification of the type of nutrient being released into the supernatant, this figure was found to be very valuable in building up an overall picture of the enzymatic breakdown of particles in the meal.

4.2. Erosion of large food particles

The release of nutrients into the supernatant is essentially governed by the disappearance of the small particles caused by their much greater surface exposure to digestive enzymes. For this reason, the results in Fig. 2 were of very limited use in providing information on the behaviour of the largest particles. The monitoring of the morphological evolution of large cheese (Fig. 4C and 6) and bread crust (Fig. 3D and 4B) particles by MRI in the course of digestion therefore provided highly useful data to complement classical chemical analyses.

Results showed a slow and linear decrease in the volume of the largest cheese particles throughout digestion (Fig. 4C). This is typical of surface, as opposed to bulk, erosion (Tamada & Langer, 1993). Their volume was extrapolated at t = 0 from the plots in Fig. 4C (~350 mm^3) and was found to be much lower than estimates based on the initial dimensions of these particles (~700 mm^3 assuming a perfect cubic shape). This discrepancy can be fully explained by the relatively low spatial resolution of UTE images compared to the size of the particles while in the present study, the voxels present at the interface between the cheese and the supernatant were not taken into account in the manual segmentation, thereby leading to a systematic underestimation of cheese particle volumes. This does not question the trends from Fig. 4C but would merit to be corrected by an increase in the spatial image resolution of future investigations.

The decrease in volume during the gastric phase (~330 mm^3 at t = 50 min down to ~260 mm^3 at t = 120 min) represent a decrease in the length of the sides of the cube of the order of only 500 μm, barely observable by the naked eye. By contrast, the sides decreased by about 1 mm in length during the intestinal phase, despite a much lower overall decrease in volume than during the gastric phase. This double erosion in terms of length reflects the much higher activity of pancreatic proteases compared to pepsin (Fig. 2B). Let us assume that the smaller cheese particles eroded the same as these largest ones, *i.e.* −0.5 and −1 mm during the gastric and intestinal phases, respectively. At the end of the gastric phase, we could expect the total disappearance of those particles that were initially smaller than 1 mm, along with a strong reduction in the size of the particles whose sides initially measured up to 2 mm (-87% in volume). When the same reasoning is applied to the intestinal phase, it can be expected that most of the particles that were initially smaller than 4 mm (80% w/w of the cheese) will disappear, while the size of the largest particles will be strongly reduced (Fig. 4C). Although not lacking in presuppositions, these estimations are largely in agreement with those from chemical analyses, *i.e.* about 34% and 75% of the proteins contained in the meal had been released in the supernatant by the end of the gastric phase and intestinal phase, respectively.

The results also showed that the crust particles also eroded slowly,

with almost all particles still floating at the surface of the digesta midway through the intestinal phase and half still present there at the end. It is possible that the disintegration of crust particles was limited because of the gentle stirring performed in our study; nevertheless, even in *in vivo* conditions, the downward propulsion of low-density food materials by peristaltic contractions may remain difficult. Indeed, the use of computational modelling has demonstrated the powerful effects of food density relative to fluid viscosity on particle trajectories in the stomach (Ferrua & Singh, 2015).

4.3. Release of lipids from cheese particles

The creaming of fat was evidenced by both MRI fat quantification (Fig. 4D) and chemical analysis (Fig. 2C). This was consistent with the occurrence of this phenomenon during gastric digestion previously observed in several MRI clinical studies (Marciani et al., 2007; Mackie et al., 2013). According to our MRI data, just over 50% of the lipids had disappeared from the deposit at t ~ 50 min under the experimental conditions chosen for the present study, while the chemical analyses suggested that the extent of creamed lipids was in the order of 30%. Although these values do not perfectly match, they remain in the same order of magnitude. The significant extent of creaming from the very outset of the experiments can only be explained by the fat having been expulsed when the cheese particles were ground in the blender and/or spread across the particle surfaces during sieving. The cheese fat thereby released then tended to cream due to its low density when immersed in the digestive fluids. The absence of variation in fat quantity measured by MRI during the second part of the gastric phase, *i.e.* when pepsin was active, seems to disagree with the progressive erosion of large cheese particles (Fig. 4C) but does appear consistent with the almost stable volume recorded for the deposit (Fig. 4B) and the slow release of free NH_2 in the supernatant (Fig. 2B). Further investigation is required to resolve these apparent discrepancies. The intestinal kinetics and the final ~ 75% loss of lipids estimated by MRI also agreed well with the overall trends obtained from the chemical analyses, with a final recovery of ~70% of creamed and solubilized lipids. The use of MRI for fat quantification is reported here for the first time, and was found to make a very valuable contribution to the general picture of the overall behaviour of the lipids present in the meal during digestion, even though its usefulness was confined to the lowest part of the vessel. Indeed, as will be discussed in section 4.5, it was not possible to use the MRI measurements to accurately monitor the increase in solubilized lipids in the supernatant nor in creamed lipids at the surface of the digesta.

4.4. Degassing and decantation of aerated food particles

Bread is a highly aerated food whose density is low (0.10–0.25 g/cm^3 according to (Zghal et al., 1999) and whose microstructure has a strong affinity for water. Consecutively to fluid absorption (Mathieu et al., 2016), the gluten-starch matrix swells, compressing the gas in the pores (Guillard et al., 2003) and, where the porosity is open (Grenier et al., 2021), expulses the gas from the crumb particles. Part of the gas, about 20% according to (Datta et al., 2007), is initially imprisoned within the gas cell walls, in the form of tiny bubbles and will be released in a slower manner, but irrevocably since imbibed walls can be easily disintegrated under friction. Because of these combined mechanisms, it was possible for us to observe visually that the crumb particles rapidly, but not instantaneously, became part of the deposit. Due to the presence of gas in the deposit, white spots in the lipid maps (Fig. 3B) were also observed in the upper part of the deposit or the supernatant over the 20 first minutes of digestion.

In dense and dry crust, the process of imbibition is slower than in crumb, lasting over the whole gastric phase (Fig. 4B). It can be assumed that breakdown of the compact gluten network began only upon the activation of the pancreatic proteases; indeed, crust particles were still floating on the upper surface of the digesta during the intestinal phase (Fig. 3D). As the crust concentrates >1/3 of dry matter in French bread, it may contribute to reduce the glycaemic index under real conditions of digestion.

The formation of a gas pocket in the stomach has been evidenced in an exemplary way by Murray et al. (2015) using skimmed-milk–based foams, but not as yet been extrapolated to other aerated foods. Our results show that bread, which is a staple food in the western diet, contributes significantly to this phenomenon and that it does so variably depending on its microstructure (different for crumb and crust).

4.5. Further improvements in quantitative MRI applied to digestion

The MRI approaches used in the present study made it possible to quantify several phenomena that occur during digestion as described above, despite some limitations. In the following, the key points of these methods, their limitations and the potential for their improvement will be discussed.

The MSE sequence was applied in the present study at relatively low magnetic field (1.5 T), with short TE and a sufficient number of points to sample relaxation curves, allowing the accurate measurement of T_2. Thanks to this parametric approach, we were able to distinguish several fractions in the digesta on the basis of their T_2 values, from about 50 min through to the end of digestion (Fig. 3A). Despite the 2D acquisition mode, the imbibition of the crust particles by the fluid could be followed in its entirety by selecting a slice thickness of the same order of magnitude as the thickness of the particles. Obviously, higher spatial resolution could help in tracking this mechanism. Unfortunately, there was a lack of quantitative information available with this protocol on the first period of gastric digestion, before the supernatant and deposit became clearly separated. In the future, however, more sophisticated strategies could be introduced. As an example, T_2 measurements in cheese could be performed using the information on the positions of cheese particles provided by the lipid maps.

In addition to the 2D T_2 mapping commonly used in food studies, we selected two 3D protocols, which allowed us to conduct quantitative study of the erosion and lipid release from the cheese particles (Fig. 4C and D, respectively). Several hypotheses were formulated regarding the quantification of the lipids. First, a lipid composition model was required. This model is based on a triglyceride molecule where certain types and relative proportions of fatty acids were assumed to be present. Despite these a priori assumptions, given that the methylene group (−CH2−) was in any case largely dominant, and that it was possible to calibrate the conversion of the signal to lipid quantities from known amounts, any inaccuracies in the model were unlikely to degrade the results. The estimated lipid signal could also be impacted by spatial variation in the sensitivity of the signal receiving coil. However, since the measurement area was relatively small and always positioned in the same location, it could be assumed that any variation from this source was negligible. It was further hypothesised that the T_1 of the cheese lipids did not vary throughout the course of digestion. Indeed, the signal from the lipids was T_1-weighted because of the short TR used to reduce the acquisition time. It would thus be possible to partially attribute the evolution of the lipid signal over time to an increase in the T_1 of the cheese particles. However, thanks to the low flip angle (15°) used for images acquisition, the signal variation regarding T_1 was relatively small. Indeed, in dedicated experiments, the T_1 of lipid in non-digested cheese at 37 °C was estimated at 260 ms. Regarding this value and the relationship between the signal and T_1, the signal loss of 32% between the gastric and the intestinal phases, would correspond, if only attributed to variation in T_1 for cheese lipids, to a T_1 increase of 700 ms, which is highly improbable given the very slight variations in T_2 for cheese meanwhile (Fig. 4A). The same conclusion could be drawn about the observation between the very beginning of the digestion process and the first measurement points for the gastric phase. Further experiments should be carried out in order to measure the evolution of fat T_1 during digestion that can distinguish the possible effects of T_1 variations from

those of lipid loss on the decrease in the lipid signal. A further issue to be addressed was the sensitivity of the estimation method to local deformations in the magnetic field used by MRI. These are found in air-matter interfaces such as those in the crumb of the bread and at the surface of the digestive fluid. It would be possible to carry out additional experiments without the bread in order to evaluate how many of the recorded disturbances were caused by tiny air bubbles. Also, the use of a sequence based on "spin echo", which is in theory less sensitive to air-matter disturbances, could partly resolve this question, although its use for the quantification of lipids would call for a parameter setting likely to make it less robust. Last, work remains to be done to improve MRI methods to quantify the increase in the solubilized lipids that are suspended in the supernatant within bile-salt mixed structures of nanometric sizes (McClements et al., 2007).

A 3D UTE sequence was selected for the analysis of cheese erosion as it allowed for the acquisition of high-resolution images (0.73 mm^3 voxel size compatible with a field of view in the order of 10 cm) in <3 min, with low sensitivity to either susceptibility artefacts (arising from the presence of air in the samples) or movement artefacts (caused by the circulation of the temperature-controlled fluid during image acquisition). However, the intensity-based segmentation of the particles was a complex process, as there was a degree of overlap in the UTE images between the T_1-weighted signal profiles of the crumb and cheese samples and the deposit. Beyond approximately 50 min, the large cheese particles were relatively easily identified by their form and position but, as described below, the method employed may be prone to error. An alternative way to distinguish the cheese particles from other food fragments would be to acquire fat selective images by adding a frequency selective water-saturation pulse before the 3D UTE acquisition pattern.

This study performed on a clinical MRI imager has demonstrated that MRI has great potential for the study of the semi-dynamic *in vitro* digestion of complex foods and also brings the possibility of *in vivo* experiments closer. The time resolution of the MRI protocol, which is suitable for the study of semi-dynamic *in vitro* digestion, obviously requires improvement for use in more realistic *in vitro* dynamic digestion experiments involving continuous fluid addition and mixing, and applications on human subjects. There are a number of available strategies to accelerate image acquisition. First, depending on the digestion phenomenon under investigation, one of the four MRI protocols set up in the present study could be prioritised and repeated throughout the course of digestion. Second, it would be possible in some cases to sacrifice a degree of spatial resolution without losing the ability to monitor the mechanism, for example, the 3D protocol for lipid quantification alone does not need highly spatially resolved measurements. Last, there are several acquisition options that allow image acquisition to be accelerated, such as parallel imaging, where a reduced amount of k-space data is collected via an array of receiver coils (Hamilton et al., 2017), or Partial Fourier imaging, which uses specific reconstruction methods to generate an entire MR image using data from only a part of *k*-space.

Finally, further studies, such as a stepwise approach where foods are measured individually would be useful for a more thorough interpretation of MRI data.

5. Conclusion

In the line of a few very recent pioneering works on single and model food, this study confirms the high potential of MRI for the *in vitro* exploration of food digestion and extends it to multi-component and multi-phase foods of realistic size. In addition to parametric T_2 imaging, two other quantitative MRI protocols (3D ultrashort echo time for morphological measurements and gradient echo for lipid quantification) were employed in an original way, demonstrating a huge potential for digestion studies. Some of the information obtained by MRI is unique in character, such as the monitoring data on the erosion of large-sized food particles, the internal gradients acquired for their imbibition of digestive fluid, and information on fat creaming. The quantitative MRI approach was reinforced by carrying out a parallel biochemical analysis of all macronutrients (starch, proteins, lipids). Overall, this approach paves the way for reliable, non-invasive, non-destructive continuous measurements to monitor *in vitro* food digestion and predict *in vivo* outcomes.

CRediT authorship contribution statement

Maja Musse: Conceptualization, Methodology, Validation, Investigation, Writing – review & editing, Visualization, Supervision, Project administration. **Steven Le Feunteun:** Conceptualization, Methodology, Validation, Investigation, Writing – review & editing, Visualization, Supervision, Project administration. **Guylaine Collewet:** Conceptualization, Methodology, Validation, Investigation, Writing – review & editing, Visualization, Supervision, Project administration. **Mattéi Ravilly:** Investigation, Visualization. **Stéphane Quellec:** Methodology, Validation, Investigation. **Jordane Ossemond:** Investigation. **Martine Morzel:** Methodology, Validation, Investigation. **Sylvain Challois:** Methodology, Validation, Investigation. **Françoise Nau:** Writing – review & editing. **Tiphaine Lucas:** Conceptualization, Methodology, Validation, Investigation, Writing – review & editing, Visualization, Supervision, Project administration.

Declaration of Competing Interest

The authors declare that they have no known competing financial interests or personal relationships that could have appeared to influence the work reported in this paper.

Acknowledgments

Part of this work has been performed using the PRISM core facility (Biogenouest, Univ Rennes, Univ Angers, INRAE, CNRS, France). Thanks go to Olivia Ménard, Tino Jamme, and Ruoxuan Deng (INRAE, Institut Agro, STLO, 35042 Rennes, France) for their technical assistance with the characterization of enzyme activities and some sample analyses.

References

Adriaensen, H., Musse, M., Quellec, S., Vignaud, A., Cambert, M., & Mariette, F. (2013). MSE-MRI sequence optimisation for measurement of bi- and tri-exponential T2 relaxation in a phantom and fruit. *Magnetic resonance imaging, 31*(10), 1677–1689.

Benders, S., & Blümich, B. (2019). Applications of magnetic resonance imaging in chemical engineering. *Physical Sciences Reviews., 4*(10).

Brodkorb, A., Egger, L., Alminger, M., Alvito, P., Assunção, R., Ballance, S., et al. (2019). INFOGEST static in vitro simulation of gastrointestinal food digestion. *Nature Protocols., 14*(4), 991–1014.

Capuano, E., & Janssen, A. E. M. (2021). Food matrix and macronutrient digestion. *Annual Review of Food Science and Technology., 12*(1), 193–212.

Chen, Y., MacNaughtan, W., Jones, P., Yang, Q., & Foster, T. (2020). The state of water and fat during the maturation of Cheddar cheese. *Food Chemistry., 303*, Article 125390.

Datta, A. K., Sahin, S., Sumnu, G., & Keskin, S. O. (2007). Porous media characterization of breads baked using novel heating modes. *Journal of Food Engineering., 79*(1), 106–116.

de Figueiredo, F. G., Ménard, O., Yu, X., Ossemond, J., Henry, G., Jardin, J., et al. (2021). In vitro dynamic digestion of model infant formulae containing lactoferrin and medium chain triacylglycerols. *Food Hydrocolloids., 118*, Article 106787.

Deng, R. X., Janssen, A. E. M., Vergeldt, F. J., Van As, H., de Graaf, C., Mars, M., et al. (2020). Exploring in vitro gastric digestion of whey protein by time-domain nuclear magnetic resonance and magnetic resonance imaging. *Food Hydrocolloids., 99*.

Deng, R. X., Seimys, A., Mars, M., Janssen, A. E. M., & Smeets, P. A. M. (2022). Monitoring pH and whey protein digestion by TD-NMR and MRI in a novel semi-dynamic in vitro gastric simulator (MR-GAS). *Food Hydrocolloids., 125*.

Fang, X. X., Rioux, L. E., Labrie, S., & Turgeon, S. L. (2016). Disintegration and nutrients release from cheese with different textural properties during in vitro digestion. *Food Research International., 88*, 276–283.

Ferrua, M. J., & Singh, R. P. (2015). Computational modelling of gastric digestion: Current challenges and future directions. *Current Opinion in Food Science., 4*, 116–123.

Floury, J., Bianchi, T., Thevenot, J., Dupont, D., Jamme, F., Lutton, E., et al. (2018). Exploring the breakdown of dairy protein gels during in vitro gastric digestion using

time-lapse synchrotron deep-UV fluorescence microscopy. *Food Chemistry., 239*, 898–910.

Freitas, D., Boué, F., Benallaoua, M., Airinei, G., Benamouzig, R., Lutton, E., … Le Feunteun, S. (2022). Glycemic response, satiety, gastric secretions and emptying after bread consumption with water, tea or lemon juice: A randomized crossover intervention using MRI. *European Journal of Nutrition, 61*(3), 1621–1636. https://doi.org/10.1007/s00394-021-02762-2

Freitas, D., & Feunteun, S. (2019). Inhibitory effect of black tea, lemon juice, and other beverages on salivary and pancreatic amylases: What impact on bread starch digestion? A dynamic in vitro study. *Food Chemistry., 297*.

Freitas, D., Le Feunteun, S., Panouillé, M., & Souchon, I. (2018). The important role of salivary α-amylase in the gastric digestion of wheat bread starch. *Food & Function., 9*(1), 200–208.

Freitas, D., Souchon, I., & Le Feunteun, S. (2022). The contribution of gastric digestion of starch to the glycaemic index of breads with different composition or structure. *Food & Function., 13*(4), 1718–1724.

Fried, M., Abramson, S., & Meyer, J. H. (1987). Passage of salivary amylase through the stomach in humans. *Digestive Diseases and Sciences., 32*(10), 1097–1103.

Goñi, I., Garcia-Alonso, A., & Saura-Calixto, F. (1997). A starch hydrolysis procedure to estimate glycemic index. *Nutrition Research., 17*(3), 427–437.

Grenier, D., Rondeau-Mouro, C., Dedey, K. B., Morel, M. H., & Lucas, T. (2021). Gas cell opening in bread dough during baking. *Trends in Food Science & Technology., 109*, 482–498.

Guillard, V., Broyart, B., Bonazzi, C., Guilbert, S., & Gontard, N. (2003). Moisture diffusivity in sponge cake as related to porous structure evaluation and moisture content. *Journal of Food Science., 68*(2), 555–562.

Hamilton, J., Franson, D., & Seiberlich, N. (2017). Recent advances in parallel imaging for MRI. *Progress in Nuclear Magnetic Resonance Spectroscopy., 101*, 71–95.

Hernando, D., Kellman, P., Haldar, J. P., & Liang, Z. P. (2010). Robust water/fat separation in the presence of large field inhomogeneities using a graph cut algorithm. *Magnetic Resonance in Medicine., 63*(1), 79–90.

Hills, B., Cano, C., & Belton, P. (1991). Proton NMR relaxation studies of aqueous polysaccharide systems. *Macromolecules., 24*(10), 2944–2950.

Hornby, H., Collado-Gonzalez, M., Zhang, X., Abrehart, N., Alshammari, M., Bakalis, S., et al. (2021). Size and number of food boluses in the stomach after eating different meals: magnetic resonance imaging insights in healthy humans. *Nutrients., 13*(10).

Iezzi, R., Locci, F., & Mucchetti, G. (2013). Cheese true density prediction by linear equations. *Journal of Food Process Engineering., 36*.

Jalabert-Malbos, M.-L., Mishellany-Dutour, A., Woda, A., & Peyron, M.-A. (2007). Particle size distribution in the food bolus after mastication of natural foods. *Food Quality and Preference., 18*(5), 803–812.

Jourdren, S., Panouillé, M., Saint-Eve, A., Déléris, I., Forest, D., Lejeune, P., et al. (2016). Breakdown pathways during oral processing of different breads: Impact of crumb and crust structures. *Food & Function., 7*(3), 1446–1457.

Le Feunteun, S., Verkempinck, S., Floury, J., Janssen, A., Kondjoyan, A., Marze, S., et al. (2021). Mathematical modelling of food hydrolysis during in vitro digestion: From single nutrient to complex foods in static and dynamic conditions. *Trends in Food Science & Technology., 116*, 870–883.

Leforestier, R., Mariette, F., & Musse, M. (2021). Impact of chemical exchange on transverse relaxation at low and moderate magnetic field strengths for sugar solutions representative of fruit tissues analyzed by simulation and MRI experiments. *Journal of Magnetic Resonance., 322*, Article 106872.

Mackie, A. R., Rafiee, H., Malcolm, P., Salt, L., & van Aken, G. (2013). Specific food structures supress appetite through reduced gastric emptying rate. *American Journal of Physiology-Gastrointestinal and Liver Physiology., 304*(11), G1038–G1043.

Marciani, L., Wickham, M., Singh, G., Bush, D., Pick, B., Cox, E., et al. (2007). Enhancement of intragastric acid stability of a fat emulsion meal delays gastric emptying and increases cholecystokinin release and gallbladder contraction. *American Journal of Physiology-Gastrointestinal and Liver Physiology., 292*(6), G1607–G1613.

Mariette, F., Collewet, G., Davenel, A., Lucas, T., & Musse, M. (2012). *Quantitative MRI in food science & food engineering* (p. 8). New Jersey, USA: John Wiley & Sons.

Mat, D. J. L., Souchon, I., Michon, C., & Le Feunteun, S. (2020). Gastro-intestinal in vitro digestions of protein emulsions monitored by pH-stat: Influence of structural properties and interplay between proteolysis and lipolysis. *Food Chemistry.*, 311.

Mathieu, V., Monnet, A. F., Jourdren, S., Panouille, M., Chappard, C., & Souchon, I. (2016). Kinetics of bread crumb hydration as related to porous microstructure. *Food & Function., 7*(8), 3577–3589.

Mayar, M., Miltenburg, J. L., Hettinga, K., Smeets, P. A. M., van Duynhoven, J. P. M., & Terenzi, C. (2022). Non-invasive monitoring of in vitro gastric milk protein digestion kinetics by H-1 NMR magnetization transfer. *Food Chemistry., 383*.

McClements, D. J., Decker, E. A., & Park, Y. (2007). Physicochemical and structural aspects of lipid digestion. In D. J. McClements (Ed.), *Understanding and controlling the microstructure of complex foods* (pp. 483–503). Woodhead Publishing Series in Food Science Technology and Nutrition.

Minekus, M., Alminger, M., Alvito, P., Ballance, S., Bohn, T., Bourlieu, C., et al. (2014). A standardised static in vitro digestion method suitable for food - An international consensus. *Food & Function., 5*(6), 1113–1124.

Morzel, M., Ramsamy, S., & Le Feunteun, S. (2023). Feasibility of using a realistic food bolus for semi-dynamic in vitro gastric digestion of hard cheese with pH-stat monitoring of protein hydrolysis. *Food Research International, 169*, 112818. https://doi.org/10.1016/j.foodres.2023.112818

Mulet-Cabero, A. I., Egger, L., Portmann, R., Menard, O., Marze, S., Minekus, M., et al. (2020). A standardised semi-dynamic in vitro digestion method suitable for food - An international consensus. *Food & Function., 11*(2), 1702–1720.

Murray, K., Placidi, E., Schuring, E. A. H., Hoad, C. L., Koppenol, W., Arnaudov, L. N., et al. (2015). Aerated drinks increase gastric volume and reduce appetite as assessed by MRI: A randomized, balanced, crossover trial. *American Journal of Clinical Nutrition., 101*(2), 270–278.

Picaud, J., Collewet, G., & Idier, J. (2016). Quantification of mass fat fraction in fish using water–fat separation MRI. *Magnetic Resonance Imaging., 34*(1), 44–50.

Salaun, F., Mietton, B., & Gaucheron, F. (2005). Buffering capacity of dairy products. *International Dairy Journal., 15*(2), 95–109.

Salelles, L., Floury, J., & Le Feunteun, S. (2021). Pepsin activity as a function of pH and digestion time on caseins and egg white proteins under static in vitro conditions. *Food & Function., 12*(24), 12468–12478.

Smeets, P. A. M., Deng, R., van Eijnatten, & Mayar, M. (2021). Monitoring food digestion with magnetic resonance techniques. *The Proceedings of the Nutrition Society, 80*(2), 148–158. https://doi.org/10.1017/S0029665120007867

Tamada, J. A., & Langer, R. (1993). Erosion kinetics of hydrolytically degradable polymers. *Proceedings of the National Academy of Sciences of the United States of America, 90*(2), 552–556.

Upreti, P., Buhlmann, P., & Metzger, L. E. (2006). Influence of calcium and phosphorus, lactose, and salt-to-moisture ratio on cheddar cheese quality: pH buffering properties of cheese. *Journal of Dairy Science., 89*(3), 938–950.

Van As, H., & van Duynhoven, J. (2013). MRI of plants and foods. *Journal of Magnetic Resonance., 229*, 25–34.

Zghal, M. C., Scanlon, M. G., & Sapirstein, H. D. (1999). Prediction of bread crumb density by digital image analysis. *Cereal Chemistry., 76*(5), 734–742.